



HAL
open science

Competing allotropes of Bi deposited on the Al₁₃Co₄(100) alloy surface

Stefania Bobaru, Emilie Gaudry, Marie-Cécile de Weerd, Julian Ledieu,
Vincent Fournée

► **To cite this version:**

Stefania Bobaru, Emilie Gaudry, Marie-Cécile de Weerd, Julian Ledieu, Vincent Fournée. Competing allotropes of Bi deposited on the Al₁₃Co₄(100) alloy surface. *Physical Review B: Condensed Matter and Materials Physics* (1998-2015), 2012, 86 (21), pp.214201. 10.1103/PhysRevB.86.214201 . hal-00974263

HAL Id: hal-00974263

<https://hal.science/hal-00974263>

Submitted on 5 Apr 2014

HAL is a multi-disciplinary open access archive for the deposit and dissemination of scientific research documents, whether they are published or not. The documents may come from teaching and research institutions in France or abroad, or from public or private research centers.

L'archive ouverte pluridisciplinaire **HAL**, est destinée au dépôt et à la diffusion de documents scientifiques de niveau recherche, publiés ou non, émanant des établissements d'enseignement et de recherche français ou étrangers, des laboratoires publics ou privés.

Competing allotropes of Bi deposited on the $\text{Al}_{13}\text{Co}_4(100)$ alloy surface

S. Bobaru, É. Gaudry, M.-C. de Weerd, J. Ledieu, and V. Fournée*

Institut Jean Lamour, UMR 7198 CNRS–Université de Lorraine, Ecole des Mines, Parc de Saurupt, 54042 Nancy Cedex, France

(Received 31 July 2012; published 5 December 2012)

The growth and stability of Bi thin films on the $\text{Al}_{13}\text{Co}_4(100)$ surface has been investigated from the submonolayer to high-coverage regime by scanning tunneling microscopy (STM) and low-energy electron diffraction (LEED) for temperatures ranging from 57 to 633 K. Initially, Bi adsorption leads to the formation of a pseudomorphic monolayer, followed by the growth of islands of different heights with increasing coverage. The in-plane structure, island height, and island morphology indicate that these islands adopt either a pseudocubic (110) or hexagonal (111) orientation normal to the surface. The (110)-oriented islands correspond to bilayer stacking (either two or four monolayers in height) while the (111)-oriented islands correspond to either three- or four-layer stacking. The in-plane orientation of (110) islands with respect to the substrate is random, while (111) islands adopt one of four possible orientations. In addition, the (111) islands show a moiré structure. The fact that Bi islands grow with either (110) or (111) orientation simultaneously on the same substrate relates to a subtle energy balance between both orientations according to *ab initio* calculations, allowing both structures to coexist. The island density dependence versus both deposition temperature and flux, their most frequent structure type, reshaping effects, and chemical reactivity of the different allotropes are also discussed in this paper.

DOI: [10.1103/PhysRevB.86.214201](https://doi.org/10.1103/PhysRevB.86.214201)

PACS number(s): 61.44.Br, 68.35.bd, 68.37.Ef

I. INTRODUCTION

Quasicrystals are intermetallic compounds with long-range order which lack the translational periodicity of normal crystals.¹ They have been discovered in more than one hundred binary and ternary systems so far. The formation of artificial single-element quasiperiodic systems has been demonstrated by using quasiperiodic surfaces as templates for metal deposition in ultra-high-vacuum conditions. This so-called pseudomorphic growth has been achieved for a limited number of cases, including elements of groups IVa (Sn, Pb) and Va (Sb, Bi)^{2–5} as well as rare gases like Xe.⁶ *Ab initio* calculations suggest that other elements could eventually lead to similar dense quasiperiodic adlayers.⁷ The pseudomorphic growth, however, is limited to the first adlayer. With increasing coverage, metal thin films tend to recover their crystalline structure. This is the case for Bi thin films on quasicrystalline surfaces, which have been extensively studied using different methods.^{2,4,8–10} The crystal structure of Bi has rhombohedral symmetry, and in the following we use rhombohedral notation. After the completion of the first pseudomorphic layer, the formation of islands consisting of bilayer stacking of Bi (110) plane was observed. Most islands exhibited a flat top and sharp edges and had a height corresponding to the stacking of four Bi (110) layers (4 ML) or a multiple.^{8,9} Two-ML islands were also observed immediately after deposition. These irregularly shaped islands tended to rearrange themselves into 4-ML islands, suggesting a special stability associated with this magic thickness of four layers.⁹ Above 5 ML, the film transformed into the Bi(111) orientation.^{8–10} A similar observation was reported for Bi deposited on Si(111)- 7×7 ¹¹ and on highly oriented pyrolytic graphite (HOPG).¹² On the Si(111)- 7×7 substrate, both 2- and 4-ML Bi (110) islands appeared to be stable on top of a wetting layer and the entire film transformed into the (111) phase once the 4-ML-thick Bi(110) slab had been completed. The driving force for the structural transformation from the (110) to the (111) phase was ascribed to a crossover at 4 ML

of the cohesive energy calculated for the two structures. In the case of HOPG, the growth occurred directly on the bare substrate without formation of a wetting layer. The Bi islands had an odd number of (110) layers (3, 5, 7, 9 ML), that is, paired layers on an intermediate monoatomic Bi layer. Again, a transformation from the (110) phase to the (111) phase was observed at larger coverages.

Here, we present a study of Bi thin films deposited on the $\text{Al}_{13}\text{Co}_4(100)$ surface characterized using scanning tunneling microscopy (STM) and low-energy electron diffraction (LEED). $\text{Al}_{13}\text{Co}_4$ is a complex metallic alloy and an approximant of decagonal quasicrystalline phases. Our results indicate the formation of a pseudomorphic wetting layer, followed by the appearance of three-dimensional (3D) islands of specific thicknesses. The islands' height and morphology, as well as their in-plane structure, indicate that both pseudocubic Bi(110) and hexagonal Bi(111) coexist on the wetting layer. The Bi(111) islands show a moiré structure resulting from the lock into registry with the substrate leading to four rotational domains, while the Bi(110) islands are randomly oriented. We also briefly discuss the film stability and its chemical reactivity towards O_2 adsorption.

The paper is organized as follows. Section II provides experimental details. All results are presented and discussed in Section III, including a brief description of the clean substrate (III A), the formation of a pseudomorphic Bi wetting layer (III B), the multilayer regime at 300 K (III C), the influence of deposition parameter on growth (III D), film stability (III E), island dynamics (III F), film reactivity (III G), and electronic structure (III H). We conclude in Sec. IV.

II. EXPERIMENTAL

The $\text{Al}_{13}\text{Co}_4$ single crystal was grown by the Czochralski method in Nancy. The initial melt composition was $\text{Al}_{84}\text{Co}_{16}$ (in at. %). The stability range of the $\text{Al}_{13}\text{Co}_4$ crystal corresponds to a Co content between 23.9 and 24.4 at. % according

to Ref. 13. The single crystal was oriented by backreflection Laue x-ray diffraction and cut perpendicular to the [100] axis. The surface was mechanically polished using diamond paste with decreasing grain size down to $0.25\ \mu\text{m}$. A clean surface was obtained by repeated cycles of 1- to 2-keV Ar^+ bombardment and annealing in the temperature range of 1070 to 1170 K under ultrahigh vacuum (base pressure 1.10^{-10} mbar). The annealing temperature of the crystal was measured using an infrared pyrometer with the emissivity set at 0.35. The quality of the surface was regularly checked by LEED, STM, and x-ray photoemission spectroscopy (XPS). STM images were recorded using a commercial Omicron VT-STM/AFM in constant-current mode and processed using the WSxM software.¹⁴ Bismuth adsorption was carried out using an electron beam evaporator with integrated flux monitor (EFM3 from Omicron). The pressure during evaporation was kept in the low 10^{-10} mbar range. The nominal thickness is given in units of monolayer equivalents (MLE) where 1 MLE corresponds to the deposition needed to form a complete pseudomorphic Bi monolayer on the substrate as seen by STM.

III. RESULTS AND DISCUSSION

A. Main features of the clean surface

The $\text{Al}_{13}\text{Co}_4$ crystal is an orthorhombic approximant with space group is $Pmn2_1$ ($oP102$) and lattice parameters are equal to $a = 0.8158\ \text{nm}$, $b = 1.2342\ \text{nm}$, and $c = 1.4452\ \text{nm}$.¹⁵ The unit cell contains 102 atoms arranged into pentagonal bipyramid clusters interconnected by glue atoms and extending along the [100] direction, which is the pseudo-ten-fold symmetry axis. The structure can also be described as the stacking of flat (F) and puckered (P) layers along the [100] direction. Earlier studies of the (100) surface based on both experimental (STM, XPS, and dynamical LEED) and *ab initio* studies using density functional theory (DFT) have shown that the surface terminates at incomplete P layers.^{16,17} The best agreement is found for the P termination models that have all 22 Al atoms per surface unit cell present, but with all 4 Co atoms per unit cell missing. Aside from these missing atoms, the surface structure is similar to that of the corresponding bulk planes, with only a small amount of relaxation in the surface layers as determined by LEED. A typical high-resolution STM image of the clean surface and the corresponding LEED pattern are shown in Figs. 1(a) and 1(b). A schematic of the Al bipentagonal features characteristic of this surface is superimposed on the image in Fig. 1(a) for illustration.

B. Formation of a pseudomorphic Bi wetting layer

Figures 1(c) and 1(d) show STM images of the surface after Bi deposition at room temperature in the submonolayer regime, for coverages of 0.15 and 0.45 MLE respectively. The formation of small protrusions homogeneous in size is observed in Fig. 1(c). Their average height with respect to the surface plane is 0.2 nm, that is, an atom high. Their apparent diameter as measured by STM is 0.8 nm, thus their real diameter must be smaller than this value due to tip convolution effects. They may correspond to single adatoms or small islands. At this stage, they are still highly mobile, as seen from the streaks in the image shown in Fig. 1(c). From the STM images, it is observed

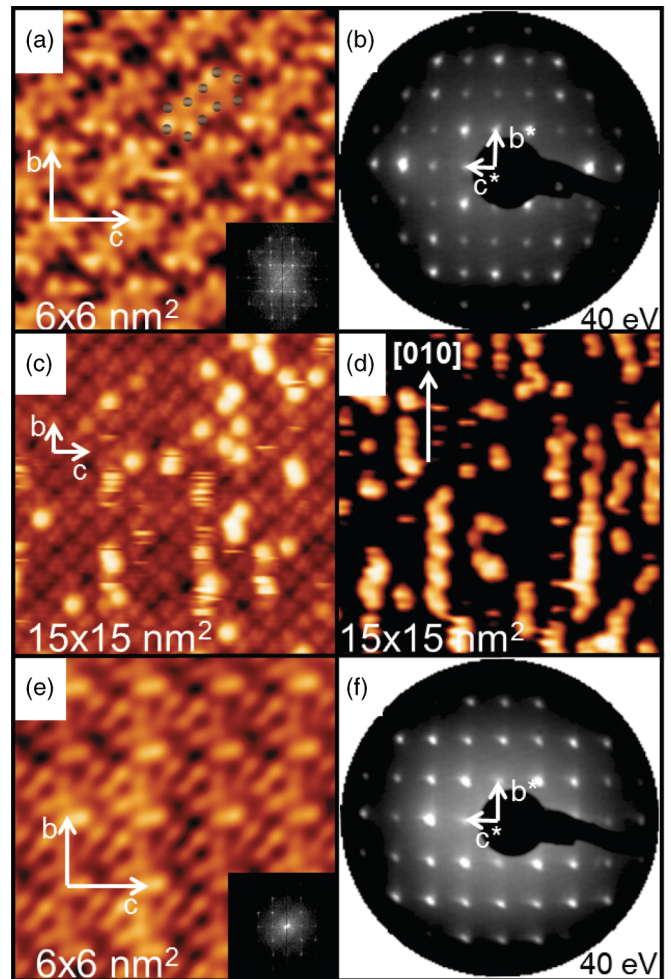


FIG. 1. (Color online) (a) STM image of the clean $\text{Al}_{13}\text{Co}_4(100)$ surface ($I_t = 0.1\ \text{nA}$, $V_b = -0.6\ \text{V}$). The unit cell and a schematic of the bipentagonal motif are superimposed on the image. Inset: Fast-Fourier transform (FFT) of the image. (b) LEED pattern of the clean $\text{Al}_{13}\text{Co}_4(100)$ surface. (c)–(e) STM images of the surface dosed with 0.15 ML (c), 0.45 ML (d), and 1 ML (e) showing the formation of small circular Bi islands (c) developing into lines extending along the [010] direction (d) and finally forming a pseudomorphic wetting layer (e) ($I_t = 0.1\ \text{nA}$, $V_b = +1\ \text{V}$). The image (e) has been Fourier filtered and the FFT is shown as an inset. (f) The LEED pattern of the surface dosed with 1 ML of Bi.

that the positions of these protrusions coincide with those of Al pentagonal motifs of the substrate highlighted in Fig. 1(a). With increasing coverage, these adatoms interconnect to form zigzagging chains extending preferentially along the [010] direction [Fig. 1(d)]. A similar row structure extending along [010] has also been reported for Pb thin films grown on the same substrate.^{18,19} Figures 1(e) and 1(f) show a typical STM image of the film and the corresponding LEED pattern after completion of the first monolayer. The film has a periodic structure with a rectangular surface unit cell of the exact same dimensions as for the substrate. The LEED pattern is also consistent with the formation of a pseudomorphic wetting layer. The detailed structure of the pseudomorphic Bi layer is not known. However, structural motifs with a distorted

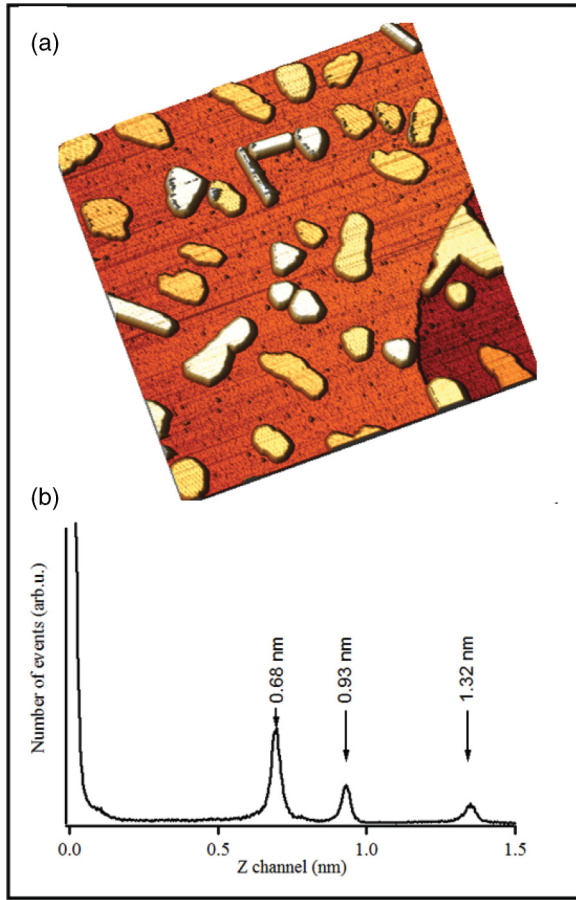


FIG. 2. (Color online) (a) 3D view of the $\text{Al}_{13}\text{Co}_4(100)$ surface dosed with 2.6 ML of Bi (STM, $I_t = 0.1$ nA, $V_b = +2$ V, 300×300 nm²). (b) Height histogram of the Bi film showing the three specific island heights.

pentagonal symmetry can be recognized in the STM image shown in Fig. 1(e). This pseudomorphic layer is quite stable and only desorbs after annealing at temperatures higher than 673 K.

C. Multilayer regime at 300 K

Figure 2(a) shows a large-scale STM image of the Bi film at a coverage of 2.6 MLE. The formation of large islands is observed, nucleating both at step edges and on terraces. Islands exhibit a variety of different shapes and can be classified according to three specific heights: S (0.68 ± 0.02), M (0.93 ± 0.02), and L (1.32 ± 0.03 nm). Measured heights are given with respect to the Bi wetting layer. They have been measured from height histograms from a large number of STM images after careful plane subtraction. One example of such height histogram is shown in Fig. 2(b). The variety of island shapes observed is illustrated in Fig. 3. The S islands are irregular in shape [Fig. 3(a)] while the M islands usually have a truncated hexagonal shape [Fig. 3(b)]. In addition, the surface of the M islands is characterized by a moiré structure. The L islands appear either as elongated rectangular structures with flat tops [Fig. 3(c)] or as truncated hexagons with a moiré structure on top, similar to M islands [Fig. 3(d)]. Because island shapes frequently reflect their crystalline structure, this

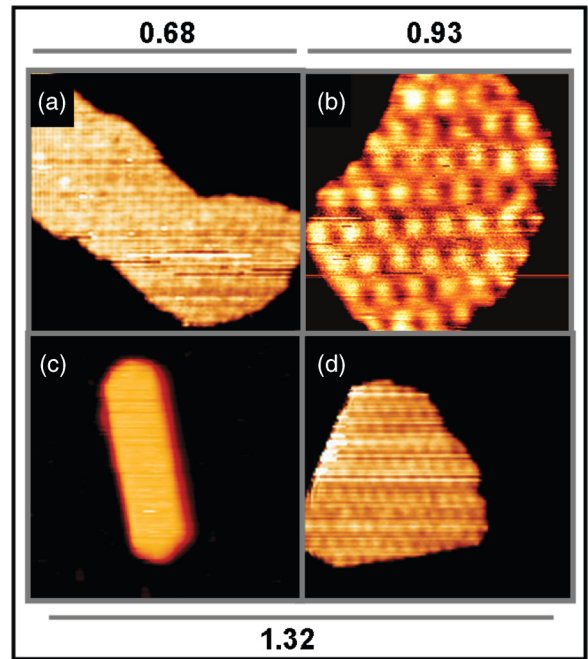


FIG. 3. (Color online) STM images of the various type of islands observed on the $\text{Al}_{13}\text{Co}_4(100)$ surface dosed with 2.6 ML of Bi [$I_t = 0.1$ nA, $V_b = +2$ V, (a) 40×40 nm², (b) 24×24 nm², (c) 40×40 nm², (d) 30×30 nm²]. Island heights are specified in nanometers.

suggests that the Bi islands can adopt different structure types during growth.

To interpret these observations, we review here the structural parameters of the three low-index surfaces of bismuth. Bulk Bi has a rhombohedral structure (space group $R\bar{3}m$, A7 arsenic structure type).^{20,21} The low-index surfaces in the rhombohedral notations are the (110), (111), and (100) surfaces and are described in Fig. 4. The (110) surface has a pseudosquare structure, whereas the last two have

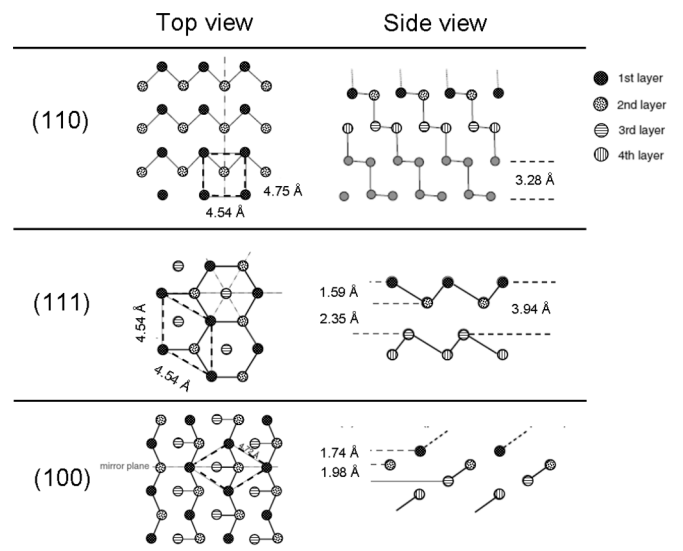


FIG. 4. Bulk truncated structure of Bi(110), Bi(111), and Bi(100) surfaces. Solid lines indicate covalent bonds within the layers. The unit cells and mirror planes are drawn as dashed lines. Adapted from Ref. 21.

TABLE I. Interlayer spacings for the three low-index surfaces of Bi (in nm).

	(110)	(111)	(100)
d_{hkl}	0.33	0.39	0.37
$2d_{hkl}$	0.66	0.78	0.74
$3d_{hkl}$	0.99	1.17	1.11
$4d_{hkl}$	1.32	1.56	1.48

pseudohexagonal structures. In bulk, each atom forms three covalent bonds with its three equidistant nearest neighbors and has three next-nearest neighbors further away. Perpendicular to the [111] direction, Bi atoms are arranged into puckered layers in which each atom is covalently bonded to its three nearest neighbors. The three next-nearest atoms are located in adjacent layers and are less strongly bonded. Therefore, no covalent bond has to be broken in order to form a Bi(111) surface. This is not the case for the Bi(100) surface in which each atom has only two covalent bonds in the plane, leaving a dangling bond at the surface. As a result, the (111) surface is preferred over the (100) orientation. The (111) surface is actually the natural cleavage plane of Bi and the preferred direction of epitaxial growth in general. The Bi(110) surface has a pseudosquare structure and contains a single mirror plane. Within the surface plane, each atom is covalently bonded to two nearest-neighbor atoms, and a third dangling bond is left at the surface. However, in the case of films with an even number of layer, it has been shown that the structure relaxes and the layers pair up, allowing the complete saturation of the dangling bonds.^{11,22} The structure of such film is similar to that of black phosphorus (orthorhombic *A17* allotrope).

The interlayer spacings for the three low-index surfaces of Bi are given in Table I. The thicknesses of S and L islands reasonably match with the thicknesses of two and four layers of Bi(110) with pseudosquare structure. Some of the L islands have a rectangular shape that is consistent with (110) orientation. The strong anisotropy of these L islands is probably related to the bond orientational order in Bi(110). The thickness of M islands is more puzzling, as it does not match with any multiples of the interlayer spacing of the low-index Bi surfaces. It could eventually be ascribed to a trilayer of Bi(110) but this possibility must be disregarded from the overall M-island shape. Their characteristic truncated hexagonal shape suggests a (111) or (100) orientation. As mentioned above, the (111) orientation is energetically favored over (100) and therefore is more likely. We also note that the thickness difference between M and L islands matches with the interlayer spacing for (111) orientation (0.39 nm). In addition, some of the L islands exhibit a truncated hexagonal shape like M islands. Therefore, this subset of L islands could be M islands having an additional puckered (111) layer on top. The thickness of M islands could thus correspond to that of three layers of Bi(111), the first one being directly in contact with the $\text{Al}_{13}\text{Co}_4$ substrate. This implies a structural modification of the wetting layer to form the first puckered (111) plane of M islands at the interface with the substrate.

Upon further deposition, the Bi islands extend laterally and the island height distribution evolves towards the L value. At about 5 MLE, the film has an average L thickness on top of

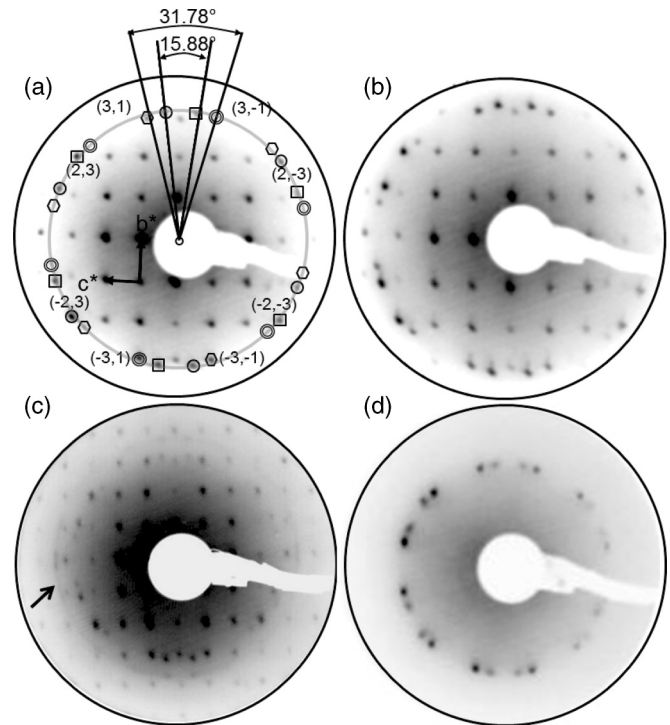


FIG. 5. LEED patterns from Bi thin films on the $\text{Al}_{13}\text{Co}_4(100)$ surface deposited at 300 K. (a) 25 eV, 2 MLE; (b) 25 eV, 6 MLE; (c) 40 eV, 4 MLE; and (d) 45 eV, 18 MLE. The ring of 24 spots corresponding to the four hexagonal domains of Bi(111) is outlined in panel (a), each domain having its own symbol. Substrate coincidence reciprocal lattice points are indicated. Rotation angles between hexagonal domains and the substrate are also noted. The diffuse ring corresponding to rotationally disordered Bi(110) domains is indicated by the arrow in panel (c).

the wetting layer. However, there are still some holes in the L-thick film which extend down to the wetting layer, together with additional islands growing on top of the L-thick film. Most of these additional islands have a triangular shape, with a step height of 0.4 ± 0.01 nm corresponding to the interlayer spacing for Bi(111) orientation. With increasing coverage, the film continues to grow in a layer-by-layer fashion, with only triangularly shaped step edges. This indicates that while the two types of structure, Bi(111) and Bi(110), compete at coverages below 5 MLE, the hexagonal structure dominates above this critical thickness. The LEED patterns of the film at various coverages are shown in Fig. 5. A ring of 24 additional spots is observed in addition to the substrate spots already at 2 MLE, and their intensity increases with increasing coverage while the substrate spots' intensity decreases. It corresponds to four hexagonal domains of Bi(111) which are orientationally ordered with respect to the substrate. The four hexagonal patterns are schematically drawn in Fig. 5(a). Two of them have their first-order spot in coincidence with either (3,1) or (3,-1) substrate spots. The other two have coincidences of reciprocal lattice point with either (2,3) or (2,-3) substrate spots. This corresponds to a momentum transfer of either 1.588 \AA^{-1} or 1.654 \AA^{-1} , giving a lattice constant of either 4.57 \AA or 4.38 \AA respectively. Compared to the bulk value of 4.54 \AA , the first set of Bi(111) domains is slightly expanded by only 0.6% while the second set is contracted by about

3.6%. Thus the two sets of orientations allow locking into registry at the interface between the Bi(111) domains and the orthorhombic substrate. Note that the two sets have unequal spot intensities. At low coverage, the domains in coincidence with either (2,3) or (2,-3) substrate spots are more intense [Fig. 5(b)] while, at higher coverage, domains in coincidence with either (3,1) or (3,-1) spots are more intense [Fig. 5(d)]. Another feature in the LEED pattern observed at intermediate coverage (below 5 ML) is the presence of a faint diffuse ring indicated by the arrow in Fig. 5(c). The radius of this ring is $k = 1.91 \text{ \AA}^{-1}$, consistent with (110) domains with interplanar distance of 3.28 Å. The lack of diffraction spots indicates the absence of orientational order of the pseudosquare islands with respect to the substrate. A similar diffuse ring has previously been reported for Bi films on the fivefold surface of the icosahedral Al-Pd-Mn quasicrystalline or on the Si(111)- 7×7 surface.^{10,11,23} The intensity of this diffuse ring depends on the fraction of the surface covered with Bi(110) islands and their size. The fraction of Bi(110) islands is certainly smaller on the Al₁₃Co₄ substrate compared to these systems, because they compete with the Bi(111) orientation already in the early stage of thin film growth. This could be the reason why this diffuse ring is so faint.

We now describe the moiré structure observed by STM on the hexagonal Bi islands. The moiré lattice is oblique and has parameters equal to $a_m = 2.86 \text{ nm}$, $b_m = 3.89 \text{ nm}$, and $\gamma_m = 68^\circ$. To understand its origin, we focus on one domain of Bi(111) having one of its first-order spots in coincidence with the (2,3) [and (-2, -3)] substrate spot as seen in the LEED pattern [square symbols in Fig. 5(a)]. The orientation of the hexagonal domain with respect to the orthorhombic substrate can be deduced from the LEED pattern. The angle between the (1,0) direction of the hexagonal lattice and the [001] direction of the substrate is 7.94° (other domains are rotated by -7.94° , $+15.89^\circ$, and -15.89° respectively). The coincidence of reciprocal lattice points is achieved through a small contraction of the Bi(111) plane to 4.38 Å. The situation is illustrated in Fig. 6, showing the simulated LEED pattern for a rotated hexagonal overlayer on the orthorhombic substrate [Fig. 6(a)] and the corresponding real space lattices superimposed [Fig. 6(b)]. The points of coincidence between the lattices are outlined as circles in Fig. 6(b) and define the oblique lattice of the moiré experimentally observed as in Figs. 6(c) and 6(d). Following the same procedure with the three other domains leads to the same moiré lattice. Thus it can be concluded that the moiré pattern is induced at the interface by the coincidence lattice.

D. Influence of the deposition temperature on growth

The growth of Bi thin films has been investigated at low temperature (57 K) by STM. Compared to room-temperature growth, the island density is much higher, increasing from approximately $5.10^{-4}/\text{nm}^2$ at 300 K [Fig. 7(a)] to $10^{-2}/\text{nm}^2$ at 57 K for the same flux $F = 10^{-3} \text{ ML/s}$ [Fig. 7(b)] and a coverage of 2.6 MLE. With increasing coverage and compared to room-temperature growth, the film height distribution evolves more rapidly towards the L thickness, with a larger fraction of the L-thick film corresponding to Bi(110) pseudocubic domains as revealed by the island shapes [Fig. 7(c)]. Close to 5 MLE, the homogeneity of the film is reflected by the

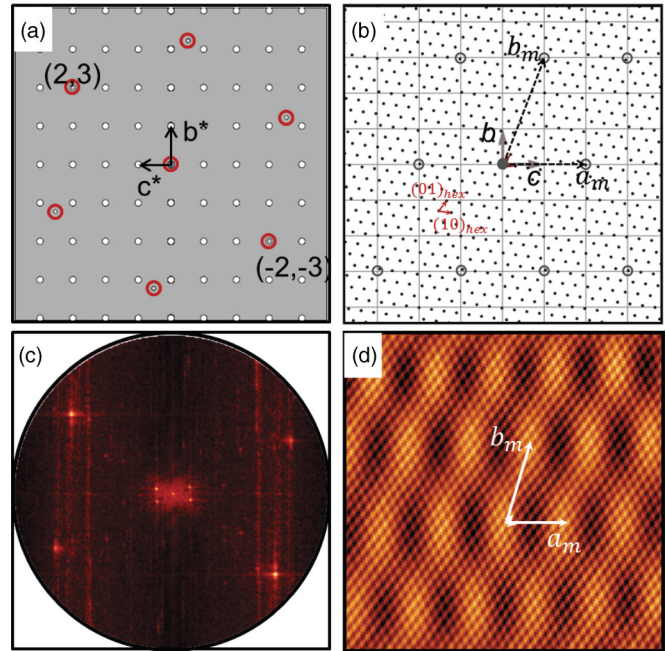


FIG. 6. (Color online) (a) Calculated LEED pattern for an hexagonal overlayer with parameter $a_{hex} = 4.38 \text{ \AA}$ rotated by 7.94° on top of the orthorhombic substrate. The (2,3) and (-2, -3) spots are coincidence reciprocal lattice spots. (b) Superposition of the real space lattices. Empty circles indicate coincidence sites which define the oblique moiré lattice, with lattice parameters $a_m = 2.86 \text{ nm}$, $b_m = 3.89 \text{ nm}$, and $\gamma_m = 68^\circ$. Panels (c) and (d) show FFT and high-resolution STM images ($15 \times 15 \text{ nm}^2$) of the Bi film, showing both the hexagonal lattice and the oblique moiré as in panel (b).

limited number of holes exposing the wetting layer and of islands growing prior to the completion of the film. Above this coverage, the film continues to grow mostly in a layer-by-layer fashion with triangular islands and step edges characteristic of the Bi(111) structure, similar to what is observed at room temperature. Figure 8 shows an atomically resolved STM image (tunneling current image) of the film at 5 ML recorded at 57 K, where several domains can be distinguished separated by boundaries. The moiré structure [Fig. 8(a)] and both lattices of hexagonal Bi(111) and pseudosquare Bi(110) [Figs. 8(b) and 8(c)] are clearly resolved. The lattice parameters measured by STM are consistent with bulk values. These images confirm the structural identification inferred earlier from island heights and

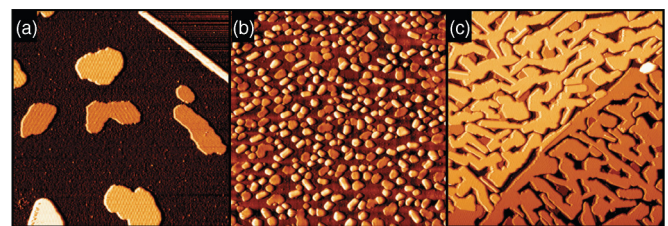


FIG. 7. (Color online) STM images of the Al₁₃Co₄(100) surface dosed with 2.6 ML of Bi ($I_t = 0.1 \text{ nA}$, $V_b = +2 \text{ V}$, $200 \times 200 \text{ nm}^2$) at 300 K (a) and at 57 K (b) using the same flux $F = 10^{-3} \text{ ML/s}$. (c) STM image of the surface dosed with 4.3 ML of Bi at 57 K ($I_t = 0.1 \text{ nA}$, $V_b = +2 \text{ V}$, $300 \times 300 \text{ nm}^2$).

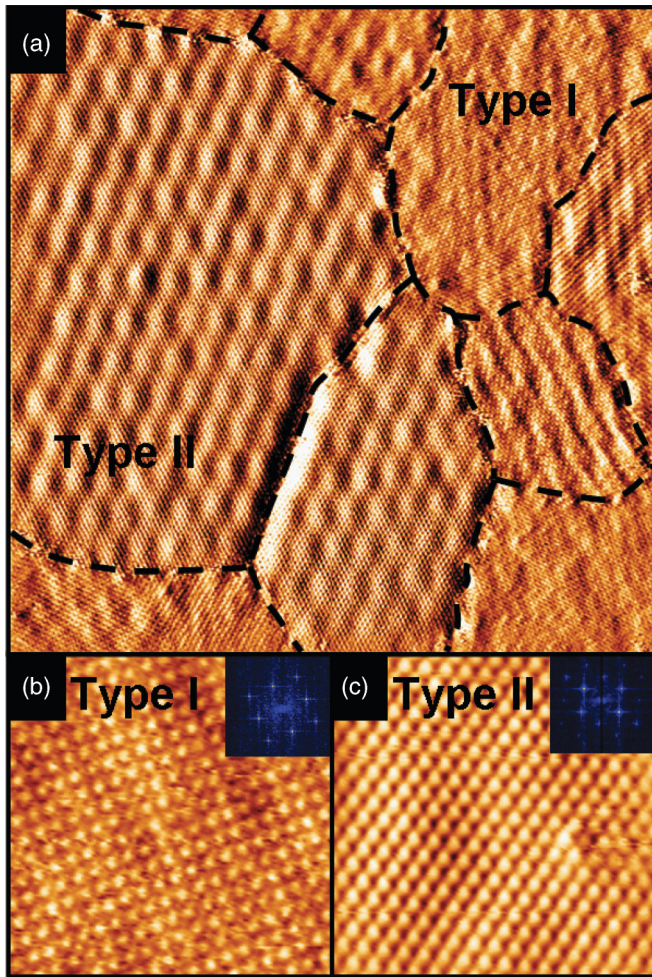


FIG. 8. (Color online) (a) Tunneling current image of the Bi film at 5 ML coverage recorded at 57 K ($I_t = 0.1$ nA, $V_b = +2$ V, 60×60 nm²). The dashed lines show the domain boundaries. Types I and II refer to the Bi(110) structure and the Bi(111) structure, respectively. Atomically resolved images of the two phases are shown in panels (b) and (c), respectively ($I_t = 0.1$ nA, $V_b = +2$ V, 7×7 nm²). Inset shows the corresponding FFT of the images.

shapes. Rotational angles measured between different Bi(111) domains match specific values imposed by the locking into registry with the substrate. These angles agree with those determined by LEED and specified in Fig. 5(a). No specific values of the rotational angles between adjacent Bi(110) domains emerge, which is consistent with the rotational disorder mentioned earlier.

We have seen that both Bi(111) and Bi(110) domains coexist on the wetting layer in the intermediate coverage regime, between 1 and 5 ML. Therefore, there must be a delicate energy balance between these two possible structures of the Bi islands. The fact that the formation of L islands with (110) structure is more favored at low-temperature deposition suggests that these L islands are unstable with respect to L islands with (111) structure.

To clarify this point, we have performed total energy calculations based on density functional theory with the generalized gradient approximation using the Vienna *ab initio* simulation package VASP.^{24,25} The projector-augmented

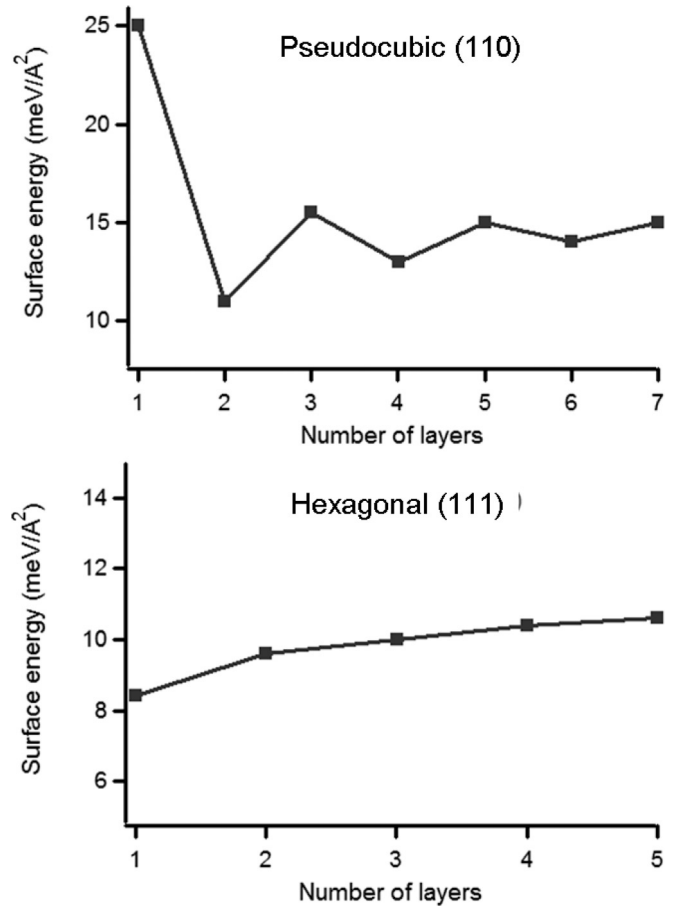


FIG. 9. Calculated surface energy for free-standing Bi(110) and (111) films as a function of the number of layers N .

wave (PAW) method^{26,27} is used to describe the interaction between the valence electrons and the ionic core. Electronic exchange and correlation is described by the generalized gradient approximation Perdew-Burke-Ernzerhof (PBE).^{28,29} The calculations were performed for free-standing Bi(110) and Bi(111) slabs of different thicknesses. The surface energy can be calculated directly by the surface free energy at zero temperature $(E_{\text{slab}} - NE_{\text{Bulk}})/(2A)$ where E_{slab} is the total energy of the slab, N is the total number of layers in the slab, E_{Bulk} is the energy per atom in the bulk crystal, and A is the surface area. We have found an oscillating behavior of the surface energy with respect to the number of layers in the slab for the (110) phase (Fig. 9). The minima of the surface energy are found for an even number of layers, supporting the bilayer growth of Bi(110) islands observed by STM. This is in agreement with earlier results by Nagao *et al.*,¹¹ who calculated the layer adsorption energy and found that films comprising an odd number of layers are unstable and evolve into films with even numbers of layers. The surface energy of free-standing Bi(111) slabs of N layers is always lower than that of Bi(110) slabs of the same thickness N . However, this difference is small, especially for $N = 2$ and 4. Therefore, it is not surprising that the two structures compete at low coverage. We stress that these calculations are only indicative since they consider free-standing films at 0 K and thus do not take into account interfacial effects or other entropic effects at $T \neq 0$ K.

However, the experiments indicate that interface does play a role as Bi growth depends on interface. Further improvements would require us to consider very large slabs consisting of a sufficient number of substrate planes with the Bi layers on top and would imply developing a structure model for the Bi wetting layer, which is beyond the scope of the present paper.

Figure 10(a) shows an STM image of the film deposited at 57 K for a coverage of 5.5 ML. At this stage, the L-thick slab is almost completed. Most islands appearing on top of the L slab have the anisotropic shapes characteristic of the Bi(110) structure and are either one or two bilayers in height. Therefore, at this stage, most of the film has the (110) structure. Figure 10(b) shows the same surface after room-temperature annealing overnight. A drastic change in the film morphology is observed. Clearly, annealing induces grain coalescence, resulting in a lower number of larger grains. Most of the surface in Fig. 10(b) is covered by a Bi slab of thickness equal to $1.74 \pm 0.03 \text{ nm} \sim L + d_{111}$. The presence of this additional (111) layer implies that most of the film has transformed from the pseudocubic to the hexagonal form upon annealing. At the bottom of the image and in the upper right corner, there is still a small fraction of the surface covered by a L-thick slab. The large holes in the film extending down to the wetting layer form as a result of this massive transformation. This transformation upon annealing is in agreement with the DFT calculations presented above.

E. Stability of the Bi thin films

The 4-ML-thick Bi film corresponding to the LEED pattern in Fig. 5(c) has been annealed gradually to test its stability. The diffuse ring corresponding to the Bi(110) domains disappear after a short annealing at 440 K. The diffraction spots corresponding to Bi(111) domains disappear after annealing at 528 K. This is in agreement with earlier reports on Bi thin film grown on quasicrystalline surfaces showing that the multilayer desorbs at about 523 K.⁹ The Bi pseudomorphic layer appears to be stable up to about 633 K, a temperature comparable to that found for the Bi or Pb wetting layer on quasicrystalline surfaces.

F. Dynamics of Bi islands

We have observed that Bi islands evolve with time and tend to reshape into islands of larger heights at room temperature. This is illustrated in Fig. 10 for both isolated hexagonal and pseudocubic islands. The L island at the bottom of Fig. 11(a) consists of two bilayers of Bi(110) and reshapes into an (L + S) island consisting of three bilayers of Bi(110) in Fig. 11(b). The surface of the island has been reduced concurrently by about a third; therefore the reshaping does not require extra adatoms. The time elapsed between these two images is about 25 min. Similarly, the hexagonal islands attached at step edge in Fig. 11(c) has an L height except for its top part, which has an M height. Upon scanning the same area, the island reshapes into a uniform hexagonal L island [Fig. 11(d)]. The time elapsed between these two images is about 50 min. In both cases, the Bi film had been prepared several hours before STM acquisition, as much as 14 h in some cases. This suggests that island reshaping might

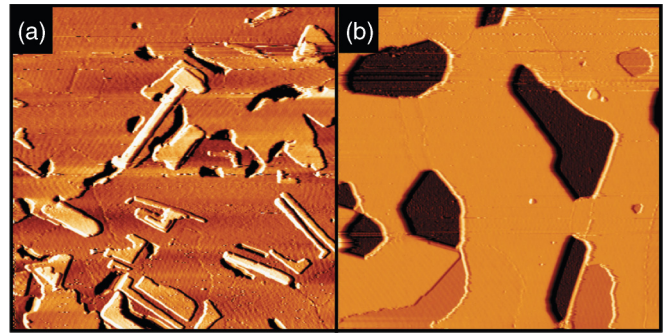


FIG. 10. (Color online) STM images of the Bi film at 5.5 ML coverage deposited at 57 K (a) and after annealing to room temperature (b) ($I_t = 0.1 \text{ nA}$, $V_b = +2 \text{ V}$, $200 \times 200 \text{ nm}^2$).

be induced by the STM tip during scanning. No structural change, from (110) to (111) or vice versa, has been observed under scanning. We also note that the hexagonal islands in Figs. 11(c) and 11(d) have a more regular shape than those in Fig. 7(a). Both films were grown under similar conditions, but the time elapsed before STM acquisition was longer in the case of Fig. 11, which could explain this difference.

G. Chemical reactivity of the Bi thin films

In the low-coverage regime (below 5 MLE), three types of structure of Bi with different properties coexist at the surface. We have investigated the chemical reactivity of the Bi film towards oxygen adsorption. For this purpose, a thin film has been prepared by deposition of 1.6 ML of Bi on the $\text{Al}_{13}\text{Co}_4(100)$ surface at room temperature and then exposed to O_2 at a pressure of 10^{-8} mbar in the STM chamber. The

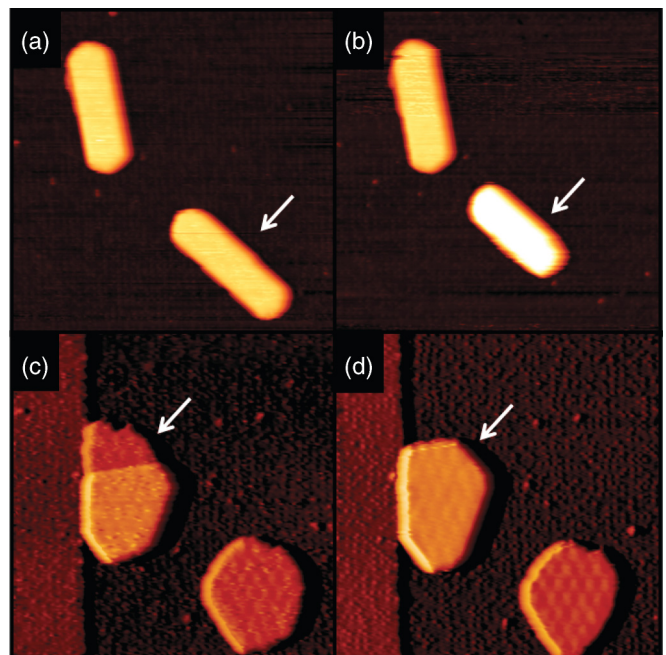


FIG. 11. (Color online) STM images illustrating the reshaping of both Bi(110) [panels (a) and (b)] and Bi(111) [panels (c) and (d)] islands at 300 K (2.6 ML coverage, $I_t = 0.1 \text{ nA}$, $V_b = +2 \text{ V}$). Panels (a) and (b): $70 \times 70 \text{ nm}^2$; panels (c) and (d): $60 \times 60 \text{ nm}^2$.

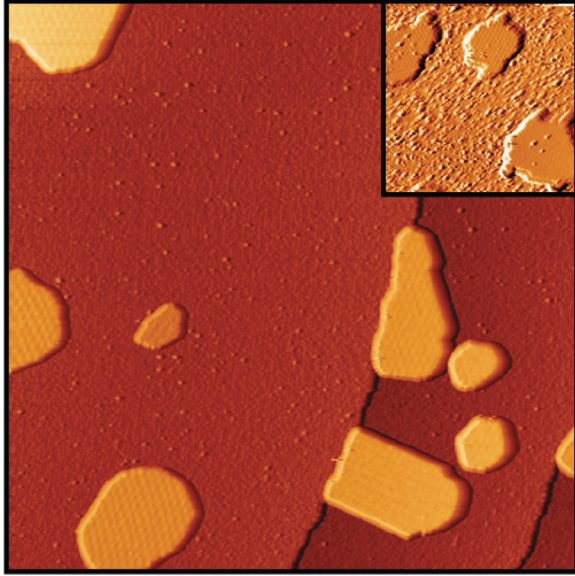


FIG. 12. (Color online) STM image of a 2.6-ML-thick Bi film on the $\text{Al}_{13}\text{Co}_4(100)$ surface and exposed to 400 L of O_2 . Oxygen adsorption is manifested by the appearance of protrusions on the wetting layer ($I_t = 0.1$ nA, $V_b = +2$ V, 200×200 nm 2). Inset: STM image in the derivative mode of the same surface exposed to about 10 000 L in $p\text{O}_2 \sim 10^{-4}$ mbar range ($I_t = 0.1$ nA, $V_b = +2$ V, 130×130 nm 2).

surface does not react very much with O_2 . Evidence for oxygen adsorption only appears after dosing several tens of Langmuir. Figure 12 shows an STM image of the film after it had been exposed to 400 L. Protrusions, related to protrusion O_2 adsorption, can only be distinguished on the pseudomorphic layer. They do not appear on top of Bi islands, independently of their structure, either S- or L-(110) or M- or L-(111) types. The pseudomorphic Bi layer is thus much more reactive compared to Bi(110) and Bi(111) surfaces. The image in the inset of Fig. 12 has been recorded after exposing the surface to more than 10 000 L in the $p\text{O}_2 \sim 10^{-4}$ mbar range. Even after such high dosing, only a few protrusions attributed to oxygen adsorption can be seen on Bi islands. Most oxygen adsorption takes place on the Bi wetting layer.

H. Scanning tunneling spectroscopy

Tunneling I(V) spectra have been recorded at room temperature on the clean substrate and on top of the various island types. The resulting normalized differential conductance curves $(dI/dV)/(I/V)$ are displayed in Fig. 13. Each curve represents the average over more than a thousand individual spectra. Each of these spectra is different, with specific features indicated by ticks in Fig. 13 that are characteristic of the island type. For the clean surface, the spectrum shows a broad minimum of the density of states (DOS) located approximately at the Fermi level E_F . This is consistent with the pseudogap expected from calculations performed within the density-functional theory (DFT) framework for the bulk structure.¹⁶ Surface DOSs have been calculated by Krajčí *et al.* for different surface termination models, including the F and P surface terminations as well as an incomplete P -layer termination.³⁰ This still differs from the model that provides

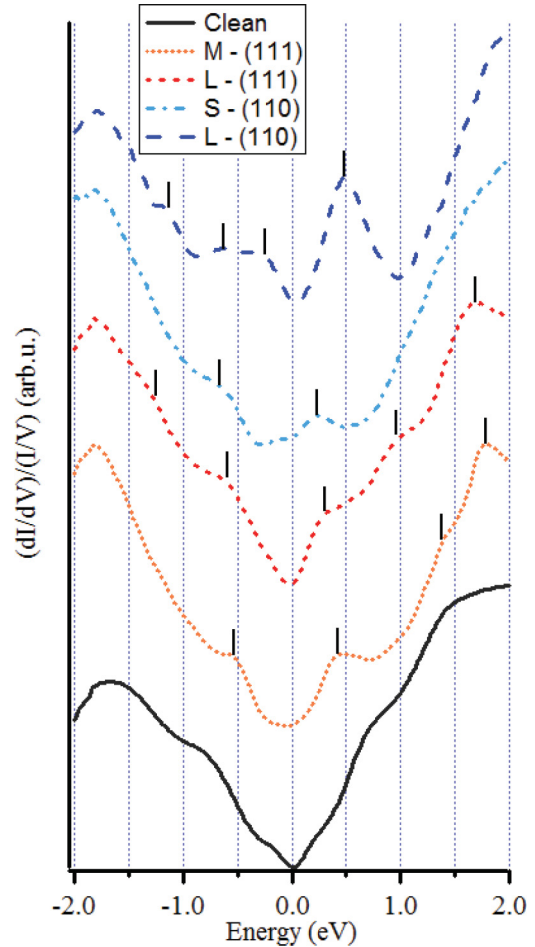


FIG. 13. (Color online) Normalized differential conductance curves $(dI/dV)/(I/V)$ recorded at 300 K on the clean substrate and on the various island types.

the best agreement with experimental results obtained on this particular sample as detailed in Ref. 17 (see Sec. III A). One important difference is the presence of some of the Co atoms in the models used for DFT calculations.³⁰ These calculations show the partial filling of the pseudogap by Co states due to a shift of the d band towards lower binding energies at the surface. However, our experiment suggests that the pseudogap is still present at the surface. In other words, the STS results are an indirect confirmation of the absence of Co atoms within the topmost surface layer of our sample.

The spectra recorded on M- and L-(111) islands present a dip in the density of states around E_F and two peaks at approximately -0.5 eV and $+0.4$ eV for M islands and -0.6 eV and $+0.3$ eV for L islands. Similar features were observed by Yaginuma *et al.* in scanning tunneling spectroscopy (STS) spectra taken from a Bi(111) film (17 layers thick) formed on Si(111)- 7×7 .³¹ These spectral features were found to be almost independent of the film thickness (10 to 25 layers) and were thus ascribed to surface states rather than to quantum well states. By comparing their low-temperature STS data with calculated DOS, the authors could ascribe these two features as originating from spin-orbit split surface-localized states inside the projected bulk band gaps. An additional feature in the vicinity of the Fermi level was also observed

both experimentally and in the calculated DOS, which was attributed to one surface-state band. This feature is not identified in our spectra, either because it is not present in three- or four-layer-thick islands or because it is smeared out due to the lower resolution inherent to room-temperature STS measurements. Surface states near the Fermi level increases the metallic character of the Bi film, compared to bulk Bi, which is a semimetal. The spectrum recorded on S-(110) islands has spectral features at approximately -0.7 eV and $+0.23$ eV and do not show clear minimum of the DOS at E_F . The spectrum recorded on L-(110) islands has spectral features at approximately -1.25 eV, -0.25 eV, -0.63 eV, and $+0.5$ eV. A dip in the DOS around E_F is also observed. The electronic properties of Bi thin films have been investigated by first-principle calculations for both (111) and (110) orientations by Koroteev *et al.*³² and compared to low-temperature STS measurements on Bi thin films grown on the Si(111)- 7×7 surface.³¹ It is found that films consisting of an odd number of Bi(110) layers with A7 structure show metallic behavior due to p_z band crossing E_F while films with an even number of layers are semiconducting because p_z states form bonding and antibonding bands which are widely split around E_F as a result of the layer-pairing mechanism. However, in the A17 structure allotrope, the films are found to be weakly metallic, with a reduced DOS at E_F . Our STS data can only be partly explained by these calculated DOSs, because room-temperature measurements imply significant broadening of the measured DOS together with uncertainties related to the Tersoff-Hamann approximation.

IV. CONCLUSION

The growth of Bi thin films on the $\text{Al}_13\text{Co}_4(100)$ surface has been investigated by STM and LEED from submonolayer to high coverage regimes. It is found that the first wetting layer adopts the complex orthorhombic structure of the substrate, in

a way similar to what has been reported earlier for Bi thin films grown on quasicrystalline surfaces. At higher coverages, Bi islands of specific heights develop. Contrary to previous observations, both Bi(110) and (111) phases coexist for $1 \leq \theta \leq 5$ MLE. The two-layer and four-layer Bi(110) islands compete with the three-layer and four-layer Bi(111) islands. The formation of the (111) phase is kinetically limited using low T deposition (or high flux). We also found that the formation of the (111) phase implies some reordering in the interfacial pseudomorphic layer. For thicker films ($\theta \geq 5$ MLE), the entire film adopts the (111) structure which, according to the DFT calculations, has the lowest surface energy. The exact critical coverage at which the transition takes place depends on the deposition parameters. Finally, the DFT calculations show that the surface energy of free-standing Bi(110) slabs is significantly lower for bilayers compared to an odd number of layers. Therefore, these islands with “magic heights” are certainly stabilized through the layer-pairing mechanism to avoid dangling bonds rather than by quantum size effects (QSEs), which are generally small in magnitude. This is line with a recent report by Han *et al.*,³³ who performed a simple electron gas model analysis indicating the possibility of QSE for free-standing Bi(110) films with a trilayer oscillation pattern ($3.d_{111} \approx 5.\lambda_F$). Considering that QSE effects are generally weak, it is unlikely that such an effect for three-layer Bi(110) could counterbalance the energy gained associated with the layer-pairing mechanism for two-layer and four-layer Bi(110).

ACKNOWLEDGMENTS

The Agence Nationale de la Recherche (ANR-08-BLAN-0041-01) and the Région Lorraine are acknowledged for their financial support.

*Corresponding author: vincent.fournée@mines.inpl-nancy.fr

¹D. Shechtman, I. Blech, D. Gratias, and J. W. Cahn, *Phys. Rev. Lett.* **53**, 1951 (1984).

²K. J. Franke, H. R. Sharma, W. Theis, P. Gille, P. Ebert, and K. H. Rieder, *Phys. Rev. Lett.* **89**, 156104 (2002).

³J. Ledieu, L. Leung, L. H. Wearing, R. McGrath, T. A. Lograsso, D. Wu, and V. Fournée, *Phys. Rev. B* **77**, 073409 (2008).

⁴J. A. Smerdon, J. K. Parle, L. H. Wearing, T. A. Lograsso, A. R. Ross, and R. McGrath, *Phys. Rev. B* **78**, 075407 (2008).

⁵J. Ledieu, M. Krajčič, J. Hafner, L. Leung, L. H. Wearing, R. McGrath, T. A. Lograsso, D. Wu, and V. Fournée, *Phys. Rev. B* **79**, 165430 (2009).

⁶S. Curtarolo, W. Setyawan, N. Ferralis, R. D. Diehl, and M. W. Cole, *Phys. Rev. Lett.* **95**, 136104 (2005).

⁷M. Krajčič and J. Hafner, *Phys. Rev. B* **77**, 134202 (2008).

⁸V. Fournée, H. R. Sharma, M. Shimoda, A. P. Tsai, B. Ůnal, A. R. Ross, T. A. Lograsso, and P. A. Thiel, *Phys. Rev. Lett.* **95**, 155504 (2005).

⁹H. R. Sharma, V. Fournée, M. Shimoda, A. R. Ross, T. A. Lograsso, P. Gille, and A. P. Tsai, *Phys. Rev. B* **78**, 155416 (2008).

¹⁰J. A. Smerdon, N. Cross, V. R. Dhanak, H. R. Sharma, K. M. Young, T. A. Lograsso, A. R. Ross, and R. McGrath, *J. Phys.: Condens. Matter* **22**, 345002 (2010).

¹¹T. Nagao, J. T. Sadowski, M. Saito, S. Yaginuma, Y. Fujikawa, T. Kogure, T. Ohno, Y. Hasegawa, S. Hasegawa, and T. Sakurai, *Phys. Rev. Lett.* **93**, 105501 (2004).

¹²P. J. Kowalczyk, O. Mahapatra, D. N. McCarthy, W. Kozłowski, Z. Klusek, and S. A. Brown, *Surf. Sci.* **605**, 659 (2011).

¹³P. Gille and B. Bauer, *Cryst. Res. Technol.* **43**, 1161 (2008).

¹⁴I. Horcas, R. Fernandez, J. M. Gomez-Rodriguez, J. Colchero, J. Gomez-Herrero, and A. M. Baro, *Rev. Sci. Instrum.* **78**, 013705 (2007).

¹⁵J. Grin, U. Burkhardt, M. Ellner, and K. Peters, *J. Alloys Compd.* **206**, 243 (1994).

¹⁶R. Addou, E. Gaudry, Th. Deniozou, M. Heggen, M. Feuerbacher, P. Gille, Yu. Grin, R. Widmer, O. Gröning, V. Fournée, J. M. Dubois, and J. Ledieu, *Phys. Rev. B* **80**, 014203 (2009).

¹⁷H. Shin, K. Pussi, É. Gaudry, J. Ledieu, V. Fournée, S. Alarcón Villaseca, J.-M. Dubois, Yu. Grin, P. Gille, W. Moritz, and R. D. Diehl, *Phys. Rev. B* **84**, 085411 (2011).

- ¹⁸R. Addou, A. K. Shukla, S. Alarcón Villaseca, É. Gaudry, Th. Deniozou, M. Heggen, M. Feuerbacher, R. Widmer, O. Gröning, V. Fournée, J.-M. Dubois, and J. Ledieu, *New J. Phys.* **13**, 103011 (2011).
- ¹⁹S. Alarcón Villaseca, J.-M. Dubois, and É. Gaudry, *Internat. J. Quantum Chem.* **13** (2012).
- ²⁰F. Jona, *Surf. Sci.* **8**, 57 (1967).
- ²¹Ph. Hofmann, *Prog. Surf. Sci.* **81**, 191 (2006).
- ²²M. Saito, T. Ohno, and T. Miyazaki, *Appl. Surf. Sci.* **237**, 80 (2004).
- ²³S. Yaginuma, T. Nagao, J. T. Sadowski, M. Saito, K. Nagaoka, Y. Fujikawa, T. Sakurai, and T. Nakayama, *Surf. Sci.* **601**, 3593 (2007).
- ²⁴G. Kresse and J. Furthmüller, *Phys. Rev. B* **54**, 11169 (1996).
- ²⁵G. Kresse and J. Furthmüller, *Comput. Mater. Sci.* **6**, 15 (1996).
- ²⁶P. E. Blöchl, *Phys. Rev. B* **50**, 17953 (1994).
- ²⁷G. Kresse and D. Joubert, *Phys. Rev. B* **59**, 1758 (1999).
- ²⁸J. P. Perdew, K. Burke, and M. Ernzerhof, *Phys. Rev. Lett.* **77**, 3865 (1996).
- ²⁹J. P. Perdew, K. Burke, and M. Ernzerhof, *Phys. Rev. Lett.* **78**, 1396 (1997).
- ³⁰M. Kražčí and J. Hafner, *Phys. Rev. B* **84**, 115410 (2011).
- ³¹S. Yaginuma, K. Nagaoka, T. Nagao, G. Bihlmayer, Y. M. Koroteev, E. V. Chulkov, and T. Nakayama, *J. Phys. Soc. Jpn.* **77**, 014701 (2008).
- ³²Y. M. Koroteev, G. Bihlmayer, E. V. Chulkov, and S. Blugel, *Phys. Rev. B* **77**, 045428 (2008).
- ³³Y. Han, B. Ůnal, D. Jing, P. A. Thiel, J. W. Evans, and D. J. Liu, *Materials* **3**, 3965 (2010).